Cent. Eur. J. Chem. • 8(3) • 2010 • 633-638
DOI: 10.2478/s11532-010-0037-8

VERSITA

Central European Journal of **Chemistry**

Sonochemical synthesis and chracterization of Mn_3O_4 nanoparticles

Research Article

Abdulhadi Baykal[a]*, Hüseyin Kavas[b], Zehra Durmuş[a], Mine Demir[a], Sinan Kazan[c], Ramazan Topkaya[c], Muhammet S. Toprak[d]

[a]*Department of Chemistry, Fatih University, B.Çekmece, 34500 Istanbul, Turkey*
[b]*Department of Physics, Fatih University, B.Çekmece, 34500 Istanbul, Turkey*
[c]*Department of Physics, Gebze Institute of Technology, 41400 Gebze,Kocaeli, Turkey*
[d]*Functional Materials Division, Royal Institute of Technology - KTH, SE16440 Stockholm, Sweden*

Received 16 November 2009; Accepted 4 January 2010

Abstract: We report on the synthesis of Mn_3O_4 nanoparticles (NPs) using a novel sonochemical method without requiring any pH adjustment. Synthesized material was identified as tetragonal hausmannite crystal structure model of Mn_3O_4 from XRD analysis. Crystallite size was estimated from x-ray line profile fitting to be 17±5 nm. FTIR analysis revealed stretching vibrations of metal ions in tetrahedral and octahedral coordination confirming the crystal structure. TEM analysis revealed a dominantly cubic morphology of NPs with an average size of ~20 nm. Magnetic evaluation revealed a blocking temperature, T_B of 40 K above which the material behaves paramagnetic. Asymmetric coercive field is attributed to the interaction between ferromagnetic Mn_3O_4 and antiferromagnetic Mn oxide at the surface of nanoparticles.

Keywords: *Sonochemistry • Mn_3O_4 • Nanomaterials • Coercive Field • Chemical Synthesis*

1. Introduction

Mn_3O_4 as a magnetic material has gained siginificant attention due to its wide range of applications, such as high-density magnetic storage media, catalyst, ion exchange, molecular adsorption, electrochemical materials [1-5]. As a nanomaterial, Mn_3O_4 NPs with remarkbly increased surface area and different morphologies are expected to exhibit better performance in all the above-mentioned applications.

Mn_3O_4 is a transition metal oxide with the normal spinel structure. The stable room temperature phase is tetragonal hausmannite ($I4_1/amd$) with Mn^{3+} and Mn^{2+} ions occupying the octahedral and tetrahedral positions of the spinel structure, respectively. Manganese ions are placed in the tetrahedral A-sites (Mn^{2+}) and octahedral B-sites (Mn^{3+}). The oxygen octahedral is tetragonally distorted due to Jahn-Teller effect on Mn^{3+} ions [6]. Various methods including high temperature sol–gel [7], sonochemical [8], co-precipitation [9], solvothermal [10], hydrothermal [11], chemical bath deposition [12], oxidation [13,14], microwave irradiation [15] and surfactant-assisted methods [16] have been reported for its synthesis.

Sonochemical technique is an effective method to synthesize magnetic NPs. Sonochemistry arises from acoustic cavitation phenomenon, that is, the formation, growth, and collapse of bubbles in liquid medium. The sonochemical method has some advantages, including uniformity of mixing, reduction of crystal growth and morphological control. Ultrasound can also fracture agglomerates to produce a uniform composition of products. The use of ultrasound radiation during the homogeneous precipitation of the precursor is expected to reduce the precipitation time of the precursor and to ensure homogeneity of the cations in the precursor [17]. The chemical effect of ultrasound arise from acoustic cavitation phenomena, *i.e.*, formation, growth, and implosive collapse of bubbles in a liquid medium. The cavitation collapse leads to many extreme conditions, viz. extremely high temperature (>5000 K), high pressure (>20 Mpa), and very high cooling rates (10^{10} Ks^{-1}), which produce unusual chemical and physical environments [18,19] .

In this work we present a sonochemical route for the synthesis of Mn_3O_4 nanocrystals which is, to the best of our knowledge, the first report on its synthesis by this route. A detailed magnetic evaluation of the synthesized material is also presented.

* *E-mail: hbaykal@fatih.edu.tr*

2. Experimental Procedure

2.1. Synthesis

Manganese (II) chloride ($MnCl_2$), anhydrous ethanol (C_2H_5OH) used in our experiments were of analytical reagent grade and purchased from Merck. The mixed solvents of anhydrous ethanol and distilled water were prepared at a ratio of 20/80 by volume and bubbled for 30 min with Ar gas. $Mn(OH)_2$ precipitate was obtained by mixing a 0.01 M $MnCl_2$ ethanol-water solution (200 mL) without performing any pH adjustment. The most important difference between our synthetic route and others is in the selection of single reactant of $MnCl_2$ aqueous solution. The $Mn(OH)_2$ precipitate was irradiated by an ultrasonic horn (20 kHz uniform sonic waves using SONOPULS HD 2200 ultrasonic homogenizer at 50% amplitude) in open air at 50ºC for 1 h. The power of ultrasonication was 16 W cm^{-2}. After that, the wet precipitate was centrifugally separated and washed by deionized water for two times, then dried at 50ºC for 2 h. To the best of our knowledge, this method of synthesis without use of any base is novel in the synthesis of Mn_3O_4 NPs.

2.2. Characterization

X-ray powder diffraction (XRD) analysis was conducted on a Huber JSODebyeflex 1001 Diffractometer operated at 40 kV and 35mA using Cu K_α radiation (λ = 1.54178 Å).

Fourier transform infrared (FT-IR) spectra were recorded in transmission mode using a Perkin Elmer BX FT-IR infrared spectrometer. The powder samples were ground with KBr and compressed into a pellet. FTIR spectra in the range 4000–400 cm^{-1} were recorded in order to investigate the nature of the chemical bonds formed.

Transmission electron microscopy (TEM) analysis was performed using a FEI Tecnai G2 Sphera microscope. A drop of diluted sample in alcohol was dripped onto a TEM grid. Following drying, the sample was loaded into a TEM column for analysis. Particle size distribution was obtained from three micrographs by counting a minimum of 100 particles.

The thermal stability was determined by thermogravimetric analysis (TGA, Perkin Elmer Instruments model, STA 6000). The TGA thermograms were recorded for a powder sample of 5 mg at a heating rate of 10 °C min in the temperature range of 30-800°C under nitrogen atmosphere.

VSM measurements were performed by using a Quantum Design Vibrating sample magnetometer (QD-VSM). The sample was measured between ±10 kOe at room temperature and at 10 K. ZFC (zero field cooling) and FC (field cooling) measurements were carried out at 100 Oe and the blocking temperature was determined from the measurements.

3. Results and Discussion

3.1. XRD Analysis

XRD pattern of the as-synthesized Mn_3O_4 powder is shown in Fig. 1. All diffraction peaks were indexed to the tetragonal hausmannite crystal structure model of Mn_3O_4 (which are consistent with bulk value—ICDD Card no. 24-0734). No extra peaks of impurities indicating other forms of manganese oxides were detected. The mean size of the crystallites was estimated from the diffraction pattern using the line profile fitting Eq. 1 given in Wejrzanowski *et al.* [20] and Pielaszek [21]. The line profile, shown in Fig.1, is fitted for 14 peaks (112), (200), (103), (211), (004), (220), (204), (015), (312), (303), (321), (224), (116), and (400). The average crystallite

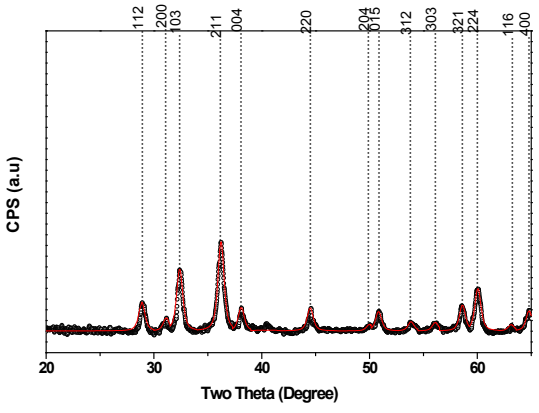

Figure 1. X-ray powder diffraction pattern (dots) and line profile fitting (solid line) for sonochemically synthesized Mn_3O_4 NPs.

size, D and σ, was estimated to be 17±5 nm.

Mn_3O_4 is a mixed oxide containing Mn ions with two different oxidation states; namely +2 and +3. This result suggests that Mn^{3+} ions are produced by the oxidation of Mn^{2+} ions during sonication which were then utilised in the formation of Mn_3O_4.

3.2. FTIR analysis

FTIR analysis was performed on the prepared sample and the spectrum is presented in Fig. 2. Two broad peaks at 3414 and 1620 cm^{-1} are assigned to O-H stretching and bending modes of adsorbed water on the surface of the Mn_3O_4 NPs. Two absorption bands observed at 621 and 512 cm^{-1} are associated with the coupling between Mn-O stretching modes of tetrahedral A- and octahedral B- sites [22-26], as expected from

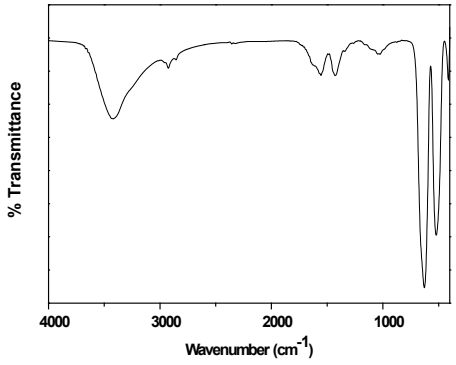

Figure 2. FTIR spectrum of sonochemically synthesized Mn_3O_4 NPs

normal spinel structure.

The CH_2 symmetric and asymmetric stretching vibrations of ethanol on the surface of Mn_3O_4 NPs lie at 2850 and 2917 cm^{-1}. The IR bands at 1055 cm^{-1} and 1455 cm^{-1}, which were not detected for the samples synthesized in aqueous solution, are attributed to the absorption of the ethanol molecules on the surface of the Mn_3O_4 NPs [27].

3.3. Thermal analysis

TGA analysis of Mn_3O_4 NPs was performed to investigate the thermal stability of as-synthesized material. A very small weight change of less than 1% (data not shown) was observed due to the adsorbed moisture and evapoartion of adsorbed alcohol on the surface, and no other changes were observed.

3.4. TEM measurements

TEM analysis was performed to investigate the morphology and size of Mn_3O_4 NPs. A typical TEM micrograph and size distribution histogram of sonochemically synthesized Mn_3O_4 NPs are given in Figs. 3a and 3b, respectively. The micrograph shows that particles are about 20 nm in diamater with close to cubic morphology and minimal agglomeration. Particle size distribution was obtained from several micrographs by counting a minimum of 200 NPs. Average particle size (D_{TEM}) was calculated using a log-normal fitting to the histograms obtained from several TEM micrographs to be 19.6 ± 0.2 nm. Crystallite size obtained from XRD is slightly smaller than the particle size calculated from TEM. This may suggest that some particles are single crystalline, and some are with polycrystalline character.

3.5. VSM Analysis

The magnetic properties of Mn_3O_4 NPs were investigated by measuring the magnetization in both zero-field-cooled (ZFC) and field-cooled (FC) modes under 50 Oe magnetic field. These two curves coincide initially and start to deviate from each other and follow different paths as the temperature decreased from 300 K to 10 K (the magnetization value does not change between 60 K and 300 K, which is omitted in the presented figure for clarity). The shape of FC and ZFC curves is the result of dipole-dipole interaction between the Mn_3O_4 NPs. As shown in Fig. 4, the variation of the magnetization in FC and ZFC mode indicates the superparamagnetic behavior. ZFC measurement was carried out as the temperature decreasing from room temperature to 10 K without any external magnetic field applied. Then, the 50 Oe magnetic field was applied during the heating process.

In both FC and ZFC curves the magnetization starts to increase sharply with decreasing temperature, and the sample shows the existence of magnetically aligned moments with and without field. It changes its magnetic charateristic at this temperature known as Curie temperature, T_c. The measured T_c for Mn_3O_4 NPs of size

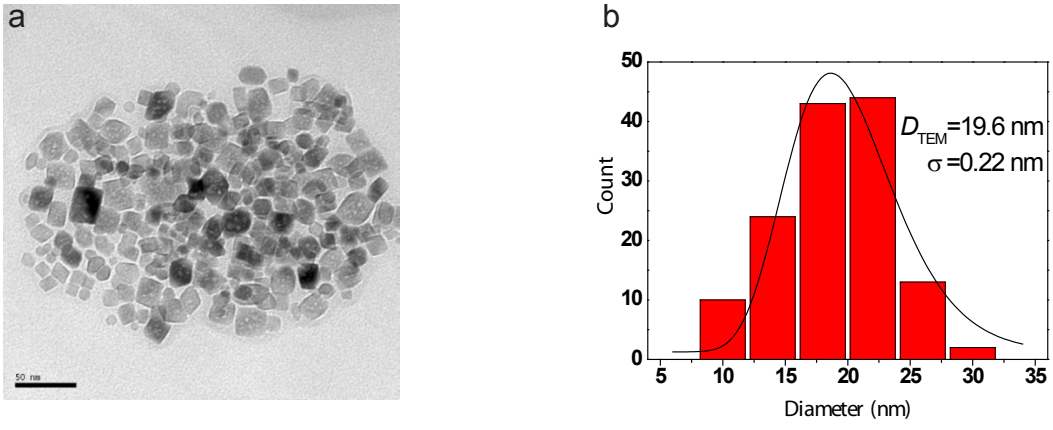

Figure 3. (a) TEM micrograph and (b) size distribution histogram of sonochemically synthesized Mn_3O_4 NPs.

19 nm is 42 K. Both Winkler *et al*. [29] and Regmi *et al*. [28] reported T_c to be 42 K for Mn_3O_4 with average size of 15 nm in diffrent studies, which is in consistency with our observations. A detailed explanation about the non-varying magnetic transition temperature for Mn_3O_4 with particle size in the range of 15-25 nm can be found in [28]. The opposite signs of first derivatives of magnetization with respect to T confirms that the magnetic phase transition is at about 42 K. Additionally, the first derivative characteristics are similar to those found in Winkler's [29] study. There are two reported anomalies [30,31] in temperature dependent magnetic characteristic of Mn_3O_4 below main magnetic phase transition at 42 K. They appear at 32 and 39 K and were attributed to the spin reorientations with the resultant ESR experiments. However, in our current study, these anamolies were not observed. As the temperature decreases, the deviation between FC and ZFC curves starts at about 41.5 K, which is called blocking temperature T_B below T_c.

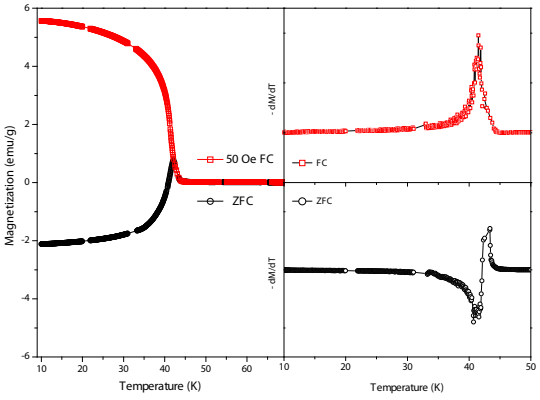

Figure 4. Zero-field-cooled (ZFC) and field-cooled (FC) magnetization curves for sonochemically synthesized Mn_3O_4 NPs measured at 50 Oe external magnetic field, and –dM/dT curves with respect to T for both FC and ZFC.

The magnetic hysterisis loops of the Mn_3O_4 at different temperatures below and above T_B in a magnetic field range of ±20 kOe are shown in Fig. 5. The saturation magnetization (M_s) was not reached, showing a maximum magnetization (M_{max}) at about 34.81 emu g^{-1} at 10 K, which is smaller than the saturation magnetization of bulk Mn_3O_4 [32,33]. The smaller Ms values in nanoparticles are generally attributed to the core-shell structure with aligned

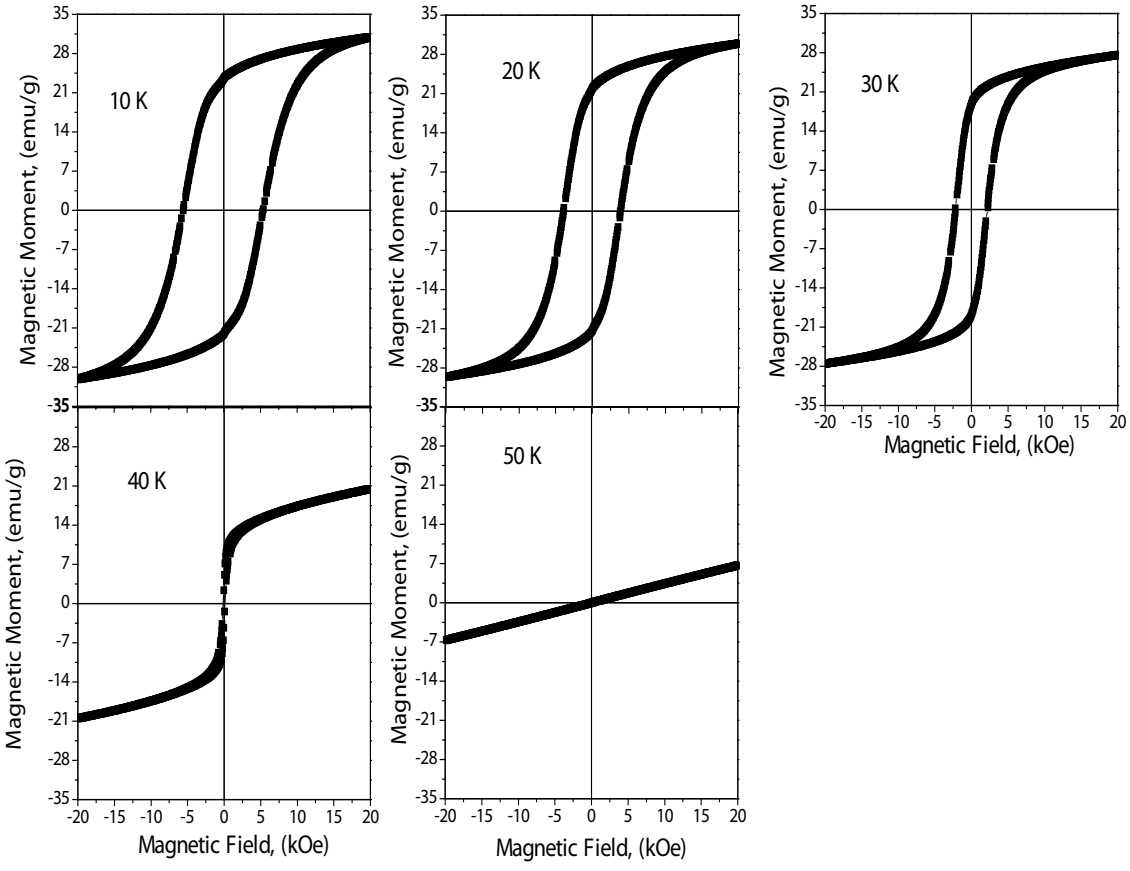

Figure 5. Magnetization (M) as a function of external magnetic field (H) at different temperatures for sonochemically synthesized Mn_3O_4 NPs

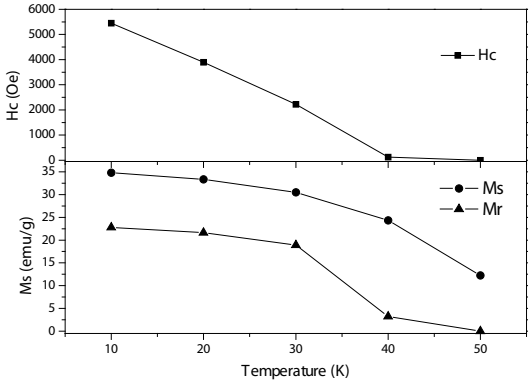

Figure 6. Temperature dependence of coercive field, saturation magnetization and remanent magnetization for sonochemically synthesized Mn_3O_4 NPs.

moments in core and canted surface moments reducing magnetization as diamagnetic structure. Moreover, non-saturated magnetization at hysteresis means co-existence of antiferromagnetic interactions with ferromagnetic interaction at low temperatures. The small coercivity and remanent magnetization at 40 K are closer to the superparamagnetic (SP) state. Additonally, the wide size distribution which allows the existence of some particles with core size of about 7 nm [29] (the treshold diameter for single domain Mn_3O_4 systems with SP property) may cause the SP like characterisitc as observed at 40 K. The magnetic hysteresis loop at 50 K (above the *Tc*) shows that Mn_3O_4 NPs behave as paramagnetic with linear *M* with respect to *H* as expected. All hysteresis show a small amount of asymmetric coercive field and this asymmetry increases with decreasing temperature.

Fig. 6 shows the temperature dependent coercive field (H_c), remanenet magnetization and saturation magnetization predicted from extrapolation of *M vs*. 1/*H* plots. The H_c decreases with increasing temperature and becomes zero above T_c. The M_s and the M_r exhibit decreasing concave down curves, characteristic of ferrimagnetic states. However, they show a sharp decrease when the temperature gets closer to T_c. This relationship between M_s and M_r indicates the phase transition at about T_c.

4. Conclusion

We have successfully synthesized Mn_3O_4 nanoparticles using a novel sonochemical method starting form a single precursor without any pH adjustment. As-synthesized material has been identified using XRD analysis as tetragonal hausmannite crystal structure model of Mn_3O_4. Crystallite size was estimated from x-ray line profile fitting to be 17±5 nm. FTIR analysis revealed stretching vibrations of metal ions in tetrahedral and octahedral coordination confirming the crystal structure as well as reflecting the ethanol coating on the surface of these NPs. TEM analysis showed a dominantly cubic morphology of NPs with an average size of ~20 nm. Comparison of particle size with crystallite size suggests that the NPs are a mixture of single crystalline and polycrystalline characters. Magnetic evaluation revealed a *Tc* of 42 K, above which the material behaves paramagnetic. The core-shell structured magnetic Mn_3O_4 nanoparticles show non-hysteric magnetization with non-saturation and increasing coercive field with decreasing temperature.

Acknowledgments

The authors are thankful to the Fatih University, Research Project Foundation (Contract no: P50020803-2) for financial support, and M.S.Toprak acknowledges the fellowship from Knut and Alice Wallenberg's Foundation

References

[1] T. Ozkaya, A. Baykal, H. Kavas, Y. Köseoğlu, M.S. Toprak, Physica B 403, 3760 (2008)
[2] K. Konstantinov, Y. Tournayre, H. K. Liu, Mater. Lett. 61, 3189 (2007)
[3] D. Pasero, N. Reeves, A. R. West, J. Power Sources 141, 156 (2005)
[4] H. Einaga, S. Futamura, J. Catal. 227, 304 (2004)
[5] X.Q. Li, L.P. Zhou, J. Gao, H. Miao, H. Zhang, J. Xu, Powder Technol. 190, 324 (2009)
[6] O.Y. Gorbenko et al., Solid State Commun. 124, 15 (2002)
[7] S. Ching, J.L. Roark, N. Duan, Chem. Mater. 9, 750 (1997)
[8] A. Askarinejad, A. Morsali, Ultrason Sonochem. 16, 124 (2009)
[9] T. Ozkaya, A. Baykal, H. Kavas, Y. Koseoglu, M.S. Toprak. Physica B 403, 3760 (2008)
[10] E. Finocchio, G. Busca. Catal Today 70, 213 (2001)
[11] Z.Y. Chang, T. Qiao, X.Y. Hu, J. Solid State Chem. 177, 4093 (2004)
[12] Y.Q. Chang, X.Y. Xu, X.H. Luo, C.P. Chen, D.P. Yu,

J. Cryst. Growth 264, 232 (2004)
[13] Z.W. Chen, J.K.L Lai, C.H. Shek, Scripta Materialia 55, 735 (2006)
[14] J. Moon, M. Awano, H. Takagi, Y. Fujishiro, J. Mater. Research 14, 4594 (1999)
[15] A. Baykal, Y. Koseoglu, M. Senel, Cent. Eur. J. Chem. 5, 169 (2007)
[16] T. Ozkaya,."Synthesis and Characterization of M3O4(M:Fe,Mn,Co) Magnetic NPs", Master Thesis, Fatih Univ., 2008, İstanbul, TURKEY
[17] H.Y. Zheng, M.Z. An, J. Alloys Compd. 459, 548 (2008)
[18] I.K. Gopalakrishnan, N. Bagkar, R. Ganguly, S.K. Kulshreshtha, Journal of Crystal Growth 280, 436 (2005)
[19] J.P. Park et al., Materials Letters 63, 2201 (2009)
[20] T. Wejrzanowski, R. Pielaszek, A. Opalinska, H. Matysiak, W. Łojkowski, K.J. Kurzydłowski, Appl. Surf. Sci. 253, 204 (2006)
[21] R. Pielaszek, Analytical expression for diffraction line profile for polydispersive powders, Appl. Crystallography, in: Proceedings of the XIX Conference, Krakow, Poland, 2003, p. 43.
[22] W. Wang, C. Xu, G. Wang, Y. Liu, C. Zheng, Adv. Mater. 14, 837 (2002)
[23] Z. Durmus, Synthesis and Characterization of Coated Magnetic Spinel Nanoparticles, Master Thesis, Fatih Univ., 2009, İstanbul, TURKEY
[24] T. Ozkaya, A. Baykal, H. Kavas, Y. Köseoglu, M.S. Toprak, Physica B 403, 3760(2008)
[25] Z. Durmus, H. Kavas, A. Baykal, M.S. Toprak, Cent. Eur. J.Chem. 7, 555 (2009)
[26] T. Özkaya, A. Baykal, M.S. Toprak, Cent. Eur. J. Chem. 6, 465 (2008)
[27] F. Dang, N. Enomoto, J. Hojo, K. Enpuku, Ultrasonics Sonochemistry 16, 649 (2009)
[28] R. Regmi, R.Tackett, G.Lawes, Journal of Magnetism and Magnetic Materials, 321, 2296 (2009)
[29] E. Winkler, R.D. Zysler, D. Fiorani, Physical Review B 70, 174406 (2004)
[30] G. Srinivasan, M.S. Seehra, Physical review B, Condensed Matter 28, 27 (1983)
[31] Z. Durmus, H. Kavas, A. Baykal, M.S. Toprak, submitted to Current applied Physics
[32] R.S. Tebble, D.J. Craik, Magnetic Materials (Academic Press, New York, 1969) 993
[33] A. Vázquez-Olmos et al., *J. Colloid Interface Sci*.